Selected for a Viewpoint in *Physics*
PHYSICAL REVIEW LETTERS

Experimental Demonstration of a Bilayer Thermal Cloak

Tiancheng Han,[1] Xue Bai,[1,2,3] Dongliang Gao,[1] John T. L. Thong,[1,3] Baowen Li,[2,3,4] and Cheng-Wei Qiu[1,3,*]

[1]*Department of Electrical and Computer Engineering, National University of Singapore, 4 Engineering Drive 3,
Singapore 117583, Republic of Singapore*
[2]*Department of Physics and Centre for Computational Science and Engineering, National University of Singapore,
Singapore 117546, Republic of Singapore*
[3]*NUS Graduate School for Integrative Sciences and Engineering, National University of Singapore,
Kent Ridge 119620, Republic of Singapore*
[4]*Center for Phononics and Thermal Energy Science, School of Physics Science and Engineering,
Tongji University, 200092 Shanghai, China*
(Received 23 August 2013; published 3 February 2014)

Invisibility has attracted intensive research in various communities, e.g., optics, electromagnetics, acoustics, thermodynamics, dc, etc. However, many experimental demonstrations have only been achieved by virtue of simplified approaches due to the inhomogeneous and extreme parameters imposed by the transformation-optic method, and usually require a challenging realization with metamaterials. In this Letter, we demonstrate a bilayer thermal cloak made of bulk isotropic materials, and it has been validated as an exact cloak. We experimentally verified its ability to maintain the heat front and its heat protection capabilities in a 2D proof-of-concept experiment. The robustness of this scheme is validated in both 2D (including oblique heat front incidence) and 3D configurations. The proposed scheme may open a new avenue to control the diffusive heat flow in ways inconceivable with phonons, and also inspire new alternatives to the functionalities promised by transformation optics.

Rendering an object invisible has been a long-standing dream for many researchers over the decades. Recently, many significant achievements of invisibility cloaking have been motivated thanks to pioneering theoretical works [1–6]. However, most cloak realizations usually require extreme constitutive parameters (inhomogeneous, anisotropic, or even singular). For the sake of feasibility, several reduced cloaks have been experimentally demonstrated at the price of giving up exactness [7–10]. Another strategy to further reduce a full cloak into something more practical is the carpet cloak [11], with several experimental realizations [12–17], which attempts to hide an object on the ground and mimic a half-infinite vacuum space. More recently, calcite crystals have been employed to fabricate carpet cloaks based on linear transformation [18,19], and one-dimensional full-parameter cloaks constructed with metamaterials have been experimentally demonstrated [20]. Readers may find more information in recent review papers [21,22]. Decoupling electric and magnetic effects, the static magnetic cloak [23,24] and the static electric cloak [25] have been experimentally realized using ferromagnetic-superconductor materials and resistor networks, respectively. In addition to manipulation of electromagnetic waves [7–25], the theoretical tool of coordinate transformation has been extended to acoustic waves [26,27] and heat flux [28–32].

On the basis of the invariance of the heat conduction equation under coordinate transformation, transforming heat transfer has provided a new method to manipulate heat flux at will [29]. Through tailoring inhomogeneity and anisotropy of conductivities (as well as specific heat and material density), transient thermal cloaking has been experimentally demonstrated recently [30,31]. In addition, steady-state thermal cloaking can be designed with only anisotropic conductivities and its construction can be further simplified by utilizing the multilayered composite approach as demonstrated both experimentally [32] and theoretically [33]. However, previous thermal cloaking approaches [30–33] usually exploit anisotropy and/or inhomogeneity, and need to be reduced for experimental realization at the price of giving up exactness. Therefore, the practical application of the thermal cloak may be limited. Surprisingly, an exact magnetostatic cloak has recently been realized using a layer of ferromagnetic material and a layer of superconductor, working at a much lower temperature (77 K) [23,24]. This motivates us to explore an exact thermal cloak with viable compositions at room temperature and higher, in particular, only employing bulk isotropic materials.

We experimentally demonstrate a bilayer thermal cloak with bulk materials, which has been theoretically validated as an exact cloak from first principles (neither a reduced cloak nor functioning only for dipolar fields). The contribution of this study is threefold. First, as the bilayer cloak does not rely on transformation optics [1–3], it can avoid the problems present in previous cloaking proposals, such as extreme parameters (inhomogeneous, anisotropic, or singular) and complicated fabrication [30–32]. Second, the proposed bilayer bulk structure which demonstrates nearly perfect performance is achieved using regular

materials, which can be readily applied. Third, the bilayer cloak is carefully investigated in both steady-state and time-dependent cases, demonstrating excellent performance in terms of heat-front maintenance and stable heat protection.

The bilayer thermal cloak, schematically illustrated in Fig. 1(a), is composed of an inner layer ($a < r < b$) and an outer layer ($b < r < c$) with conductivity of κ_2 and κ_3, respectively. The conductivity of the background is κ_b. Considering the inner layer to be a perfect insulation material, i.e., $\kappa_2 = 0$, when the external-field distortion is completely eliminated, we obtain $\kappa_3 = ((2c^3 + b^3)/2(c^3 - b^3))\kappa_b$. Rigorous analysis is provided in the Supplemental Material [34]. When we consider a two-dimensional (2D) bilayer cloak in Fig. 1(b), an analysis analogous to the 3D case can be carried out, from which the relationship is given by $\kappa_3 = (c^2 + b^2)/(c^2 - b^2)\kappa_b$. The performance of the proposed bilayer cloak has been numerically confirmed in the Supplemental Material, Fig. S1 [34].

For the measurement of thermal cloaks, one can cut the 3D bilayer sphere in Fig. 1(a) into two identical halves, and measure the temperature on the cross section. Simulation of a semi-3D bilayer cloak is shown in Supplemental Fig. S2(b), demonstrating excellent performance compared to the case with a single layer of expanded polystyrene in Fig. S2(a) [34]. Therefore, without loss of generality, we consider a 2D bilayer cloak as shown in Fig. 1(b). We choose $a = 6$, $b = 9.5$, and $c = 12$ mm. The inner and outer layers of the bilayer cloak are expanded polystyrene and Inconel 625 alloy with conductivity of 0.03 and 9.8 W/mK, respectively. For the host background material, we use a thermally conductive sealant (ACC SILICONES—AS1802) with conductivity of 2.3 W/mK. The bilayer cloak is cast in the host block with dimensions 45 (W), 45 (D), and 35 mm (H). Local heating on the left side is achieved by a heat source fixed at 60 °C, and the right side is connected to a tank filled with ice water (0 °C). The cross-sectional temperature profile is captured with a Flir i60 infrared camera. An aluminum cylinder with radius of 6 mm is placed in the central region as an object that needs to be cloaked.

Before we present the results of the bilayer cloak, we first discuss two comparison cases. The first reference structure
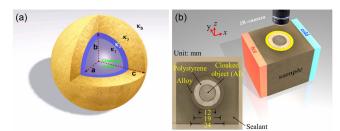
for comparison is a bare perturbation (aluminum cylinder) without bilayer cloak. The radius of the perturbation is 6 mm with the same size as the cloaking region. We cast the perturbation in the host block as described above and keep it under room temperature conditions (25 °C) for a sufficiently long time. Prior to measurement, the heat source was first heated to 60 °C, before connecting it to the left side of the cloak sample while the right side of the bulk was connected to a tank filled with ice water (0 °C). The simulated temperature profile is shown in Fig. 2(a), on which white isothermal lines are superimposed. Obviously, the presence of the perturbation completely alters the temperature profile. The high thermal conductivity of the perturbation attracts the heat flux and makes isothermal lines curve outwards both on its left and right. The corresponding measured result is shown in Fig. 2(b), which agrees well with the simulated result in Fig. 2(a). The distortion of the external thermal profile can be clearly observed.

The second reference structure is the object covered by a single layer of uniform expanded polystyrene just like that
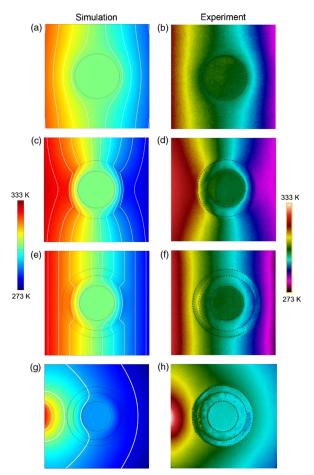

FIG. 2 (color online).   Simulated and measured temperature distributions for the steady state. (a),(b) First reference structure. (c),(d) Second reference structure. (e),(f) The proposed bilayer cloak with $a = 6$, $b = 9.5$, and $c = 12$ mm. (g),(h) The proposed bilayer thermal cloak in the presence of a point heat source, emitting cylindrical heat fronts. Isothermal lines are also represented with white color in the panel.

FIG. 1 (color online).   (a) Schematic illustration of the 3D and 2D bilayer thermal cloak with naturally available materials. (b) Experimental setup for the 2D bilayer thermal cloak. The inset shows the cross section of the experimental sample.

for the cloak; i.e., this reference structure has no outer layer. The simulated result for temperature distribution is shown in Fig. 2(c), which agrees very well with the measured thermal profile of Fig. 2(d). Obviously, though the central region is protected (thermal flux goes around the central region), the low thermal conductivity of the polystyrene repels the heat flux and makes the isothermal lines near the center of the reference structure significantly curved toward the center.

When the perturbation is wrapped by our bilayer cloak, the curved thermal profiles restore exactly without distortion as if nothing were there, as shown in Fig. 2(e). The measured result of the bilayer cloak is presented in Fig. 2(f). Clearly, the external isotherms are vertical and not distorted, as predicted in Fig. 2(e). For quantitative comparison, the simulated results in Fig. 2(e) and measured results in Fig. 2(f) along three horizontal lines ($x = -12$ mm, $x = 0$, and $x = 12$ mm) are shown in the Supplemental Material, Fig. S3. It is apparent that experiments accord well with simulations. We also examine the cloaking behavior of the bilayer cloak in the presence of a point heat-source, as shown in Figs. 2(g) and 2(h). It is obvious that experiment [Fig. 2(h)] agrees well with simulation [Fig. 2(g)], which demonstrates the effectiveness of the proposed bilayer thermal cloak in non-uniform thermal field. As a perfect thermal insulation material ($\kappa = 0$) cannot be obtained, a small amount of thermal energy will diffuse into the cloaking region and raise the temperature over a long period of time. Hence, thermal protection works only transiently (but over a decently long period as demonstrated in our thermal cloak), and such time-dependent performance has also been noted in thermal cloaks based on transformation optics [30,31]. Therefore, it is of great importance to know how long and how well the designed thermal cloak can function, i.e., the performance against time.

To examine the transient performance of the bilayer cloak, we measured the temperature distributions of the three cases in Fig. 2 at different times $t = 1$, 10, and 60 min after placing the sample into the fixed temperature field. Because the temperature of the cloaking region in steady state is close to room temperature (25 °C) when the heat source is fixed at 60 °C, it is difficult to observe the heat protection as time elapses. Thus the heat source is fixed at 80 °C for unambiguous comparison and observation. The measured results for the first reference structure are shown in the left column of Fig. 3. The strong distortion of the external thermal profile can be clearly observed, and the temperature of the object rises quickly with time. The measured results for the second reference structure are shown in the middle column of Fig. 3. The significant distortion of the external thermal profile can also be clearly observed, though the temperature of the central region now rises slowly as time elapses. The measured results for the bilayer cloak are depicted in the right column of Fig. 3. It is apparent that the cloak successfully fulfills its task in that the central region is colder than its surroundings by
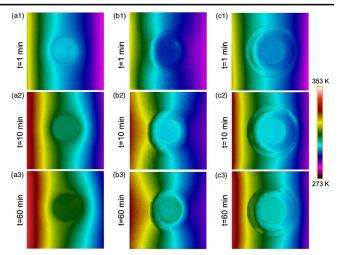

FIG. 3 (color online).   Experimental transient temperature distributions at different times $t = 1$, 10, 60 min. (a) Results for the first reference structure of Fig. 2(b). (b) Results for the second reference structure of Fig. 2(d). (c) Results for the bilayer cloak of Fig. 2(f). Obviously, both bilayer cloak and insulation coating can make the object colder than the bare object. However, only bilayer cloak can restore isothermal lines exactly without distortion as if nothing were there.

reducing the external heat flux entering the cloaking region, which can also be seen by comparing the left and right columns of Fig. 3. Furthermore, both of the front and rear temperature fronts outside the cloak are always kept nearly planar as time elapses. This transient behavior once again demonstrates the nearly perfect performance of our bilayer thermal cloak.

Simulated time-dependent temperature distributions for the three cases of Fig. 3 are given in the Supplemental Material, Fig. S4 [34]. The geometric parameters and material parameters in the simulations completely match those in the experiments. Obviously, our experiments in Fig. 3 agree very well with the simulations shown in Fig. S4. For continuous real-time observation, simulations against the evolving time have been demonstrated in the Supplemental Material, movies S1, S2, and S3, respectively [34].

It is noted that the temperature of the cloaking region is raised as time elapses due to the finite heat conductivity of the inner layer. Therefore, it is valuable for engineering applications to quantitatively examine the temperature change of the cloaking region over time. We choose $(-6, 0)$ and $(-6, 13)$ mm as observation points, corresponding to cloaking region (inside the cloak) and external region (outside the cloak), respectively, which is indicated in the upper left inset of Fig. 4. For a pure background without any perturbation, the two points should have the same temperature because they are located along the same isothermal line. Figure 4 shows the measured time-dependent temperature curves for the two test points. It is clear that the measured temperature of the cloaking region is always cooler than the external region even after

a long time (1.5 h). The temperature difference between the two test points is demonstrated in the lower right inset of Fig. 4. Obviously, the temperature outside the cloak rises much faster than the inside, especially in the first 10 min. In the long-time limit, the steady state will be reached in which the temperature of the cloaking region is constant.

In addition to our bilayer exact cloak, the other two thermal cloaking schemes have been reported including an anisotropic-inhomogeneous (AI) thermal cloak [29,30] and an anisotropic-homogeneous (AH) thermal cloak [32,33]. On the basis of transforming heat transfer [29], the transformation equation for the AI cloak can be obtained as $r = (r_2 - r_1)/(r_2 - r_0)r' + (r_1 - r_0)/(r_2 - r_0)r_2$, where r (r') is the radius in the physical (virtual) space, and r_1 (r_2) is the inner (outer) radius. Here we assume that the expansion starts from a finite small region of radius r_0 rather than exactly from a point to avoid singularity. Then the conductivities of the AI cloak can be expressed as $\kappa_r = (1 - ((r_1 - r_0)r_2/(r_2 - r_0)r))\kappa_b$ and $\kappa_\theta = \kappa_b^2/\kappa_r$, where κ_b is the conductivity of the background. The conductivities of the AH cloak are obtained [33] $\kappa_r = 2^{-n}\kappa_b$ and $\kappa_\theta = 2^n\kappa_b$, where $n > 0$.

As a fair comparison, we assume that the AI cloak and the AH cloak have the same geometrical size as the bilayer cloak, with $r_1 = 6$ and $r_2 = 12$ mm. They are cast in the host background material with conductivity of 2.3 W/mK, and an aluminum cylinder with radius of 6 mm is placed in the central region. For simplicity, we assume $r_0 = m\,r_1$, where $0 < m < 1$. Simulation results for different cloaking schemes are presented in Figs. 5(b)–5(d). Obviously, when m is small (singularity growing) and n is large (anisotropy growing) enough, the AI cloak and AH cloak perform 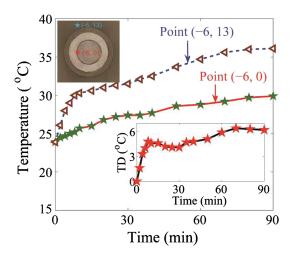nearly as perfectly as the bilayer cloak. However, the performance of the AI cloak and AH cloak is significantly degraded with the increase of m and with the decrease of n, respectively, which are confirmed in Figs. 5(e) and 5(f).

To quantitatively compare the three cloaking schemes, we calculated the temperature gradient of the cloaking region, which should be zero for ideal thermal cloak. The temperature gradient curves of the AI cloak at the central point (0,0) are demonstrated in Fig. 5(e). It is clear that temperature gradient decreases with the decrease of m, which is accompanied by increasing singularity. The temperature gradient curves of the AH cloak at the central point (0,0) are demonstrated in Fig. 5(f). It is apparent that temperature gradient decreases with the increase of n, which is accompanied with increasing anisotropy. Beyond expelling incident fields, the other function of the thermal cloak is not to distort external fields. We define temperature deformation (TD) expressed as $\mathrm{TD} = |T_{\mathrm{cloak}}|_{x=12\ \mathrm{mm}} - T_{\mathrm{background}}|_{x=12\ \mathrm{mm}}|$, in which $T_{\mathrm{background}}|_{x=12\ \mathrm{mm}}$ denotes the temperature distribution at $x = 12$ mm in Fig. 5(a) and $T_{\mathrm{cloak}}|_{x=12\ \mathrm{mm}}$ denotes the temperature distribution at $x = 12$ mm in Figs. 5(b)–5(d).
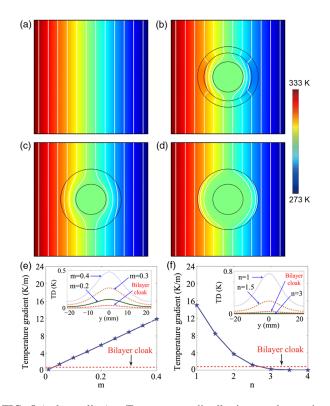

FIG. 5 (color online). Temperature distributions and quantitative comparison for different thermal cloaking schemes. (a) A pure background. (b) Bilayer thermal cloak proposed in this Letter. (c) AI thermal cloak with $m = 0.2$. (d) AH thermal cloak with $n = 3$. (e) Temperature gradient at (0,0) for AI thermal cloak with different m. The inset shows the temperature deformation of the AI thermal cloak with different m. (f) Temperature gradient at (0,0) for the AH thermal cloak with different n. Inset shows the temperature deformation of the AH thermal cloak with different n. Isothermal lines are also represented with white color in the panel.

FIG. 4 (color online). Measured time-dependent temperature for test points at $(-6,0)$ and $(-6,13)$ mm. Points $(-6\ 0)$ and $(-6,13)$ denote the cloaking region and the surrounding (external region) respectively, which have been illustrated in the upper left inset. Lower-right inset shows the temperature difference between the two test points.

Insets of Figs. 5(e) and 5(f) show the temperature deformation of the AI and AH cloak with different m and n, respectively. It can be seen that our bilayer cloak functions better than the other two thermal cloaking schemes, even using nonextreme parameters.

Comprehensive comparisons amongst these three thermal cloaking schemes indicate that the bilayer isotropic cloak functions much better than the other two cloaking schemes of AI and AH configurations. Extreme parameters might provide better performance for the AI and AH cloak, but are challenging to realize due to extreme singularities and the huge anisotropy usually required. Furthermore, the robustness of our bilayer thermal cloak has been verified against oblique heat incidence at 30° and 45°, as demonstrated in the Supplemental Material, Fig. S5 [34]. If the oblique angle approaches closer to 90°, it will not perform well, simply because now the heat is flowing along the rod.

In summary, we have experimentally demonstrated a bilayer thermal cloak with bulk materials. Our design scheme, derived directly from the conduction equation, does not rely on transformation optics [5,6], and thus avoids the problems present in previous cloaking proposals, such as extreme parameters (inhomogeneous, anisotropic, and singular) and complicated fabrication [30–32]. Also, this exact scheme is different from the scattering-cancellation technique that only diminishes the dominant order [4–6]. Finally, nearly perfect performance can be achieved employing only regular bulk materials indicating that our advanced scheme is suitable for real engineering applications.

There are three types of heat transfer: heat conduction, heat radiation, and heat convection. In heat radiation, heat is transferred by electromagnetic waves. In heat convection, heat is transferred by the mass transport. In the heat conduction case, which is the case of the thermal cloak, heat is transferred by lattice vibration, under the scope of conventional phononics. So far phononics makes use of the nonlinearity of the material or lattice to control or manipulate heat flow. Therefore, the work presented here has introduced a new dimension to the emerging field of phononics: controlling and manipulating heat flow with phonons [35].

---

*chengwei.qiu@nus.edu.sg

[1] J. B. Pendry, D. Schurig, and D. R. Smith, Science **312**, 1780 (2006).
[2] U. Leonhardt, Science **312**, 1777 (2006).
[3] V. M. Shalaev, Science **322**, 384 (2008).
[4] A. Alù and N. Engheta, Phys. Rev. E **72**, 016623 (2005).
[5] A. Alù and N. Engheta, Opt. Express **15**, 3318 (2007).
[6] A. Alù and N. Engheta, Phys. Rev. Lett. **100**, 113901 (2008).
[7] D. Schurig, J. J. Mock, B. J. Justice, S. A. Cummer, J. B. Pendry, A. F. Starr, and D. R. Smith, Science **314**, 977 (2006).
[8] B. Kanté, D. Germain, and A. de Lustrac, Phys. Rev. B **80**, 201104 (2009).
[9] S. Xu, X. Cheng, S. Xi, R. Zhang, H. O. Moser, Z. Shen, Y. Xu, Z. Huang, X. Zhang, F. Yu, B. Zhang, and H. Chen, Phys. Rev. Lett. **109**, 223903 (2012).
[10] H. Chen and B. Zheng, Sci. Rep. **2**, 255 (2012).
[11] J. Li and J. B. Pendry, Phys. Rev. Lett. **101**, 203901 (2008).
[12] R. Liu, C. Ji, J. J. Mock, J. Y. Chin, T. J. Cui, and D. R. Smith, Science **323**, 366 (2009).
[13] H. F. Ma and T. J. Cui, Nat. Commun. **1**, 21 (2010).
[14] J. H. Lee, J. Blair, V. A. Tamma, Q. Wu, S. J. Rhee, C. J. Summers, and W. Park, Opt. Express **17**, 12 922 (2009).
[15] J. Valentine, J. Li, T. Zentgraf, G. Bartal, and X. Zhang, Nat. Mater. **8**, 568 (2009).
[16] L. H. Gabrielli, J. Cardenas, C. B. Poitras, and M. Lipson, Nat. Photonics **3**, 461 (2009).
[17] T. Ergin, N. Stenger, P. Brenner, J. B. Pendry, and M. Wegener, Science **328**, 337 (2010).
[18] B. Zhang, Y. Luo, X. Liu, and G. Barbastathis, Phys. Rev. Lett. **106**, 033901 (2011).
[19] X. Chen, Y. Luo, J. Zhang, K. Jiang, J. B. Pendry, and S. Zhang, Nat. Commun. **2**, 176 (2011).
[20] N. Landy and D. R. Smith, Nat. Mater. **12**, 25 (2012).
[21] H. Chen, C. T. Chan and P. Sheng, Nat. Mater. **9**, 387 (2010).
[22] Y. Liu and X. Zhang, Nanoscale **4**, 5277 (2012).
[23] F. Gomory, M. Solovyov, J. Souc, C. Navau, J. Prat-Camps, and A. Sanchez, Science **335**, 1466 (2012).
[24] S. Narayana and Y. Sato, Adv. Mater. **24**, 71 (2012).
[25] F. Yang, Z. L. Mei, T. Y. Jin, and T. J. Cui, Phys. Rev. Lett. **109**, 053902 (2012).
[26] S. Zhang, C. Xia, and N. Fang, Phys. Rev. Lett. **106**, 024301 (2011).
[27] B.-I. Popa, L. Zigoneanu, and S. A. Cummer, Phys. Rev. Lett. **106**, 253901 (2011).
[28] C. Z. Fan, Y. Gao, and J. Huang, Appl. Phys. Lett. **92**, 251907 (2008).
[29] S. Guenneau, C. Amra, and D. Veynante, Opt. Express **20**, 8207 (2012).
[30] R. Schittny, M. Kadic, S. Guenneau, and M. Wegener, Phys. Rev. Lett. **110**, 195901 (2013).
[31] S. Narayana, S. Savo, and Y. Sato, Appl. Phys. Lett. **102**, 201904 (2013).
[32] S. Narayana and Y. Sato, Phys. Rev. Lett. **108**, 214303 (2012).
[33] T. C. Han, T. Yuan, B. W. Li, and C. W. Qiu, Sci. Rep. **3**, 1593 (2013).
[34] See Supplemental Material at http://link.aps.org/supplemental/10.1103/PhysRevLett.112.054302 for the detailed theoretical modeling, discusses the realization of three-dimensional bilayer thermal cloaks, and investigates the time-dependent and angle-dependence performance of the thermal cloak.
[35] N. B. Li, J. Ren, L. Wang, P. Hanggi, and B. Li, Rev. Mod. Phys. **84**, 1045 (2012).